

Printed Polymer-Stabilized Chiral Nematic Liquid Crystal Privacy Windows

Mengmeng Li, Waqas Kamal, Andrew C. J. Orr, Alfonso A. Castrejón-Pita, Steve J. Elston, and Stephen M. Morris*

In this paper, drop-on-demand (DoD) printing is demonstrated of polymer stabilized chiral nematic liquid crystal (PSCLC) privacy windows that can function in either a conventional mode (scattering to transparent) or reverse mode (transparent to scattering) with the application of an electric field. Inkjet printed droplets of the PSCLC mixture, with diameters of the order of 100–200 μm and sandwiched in LC layer thicknesses of $\approx 10\text{--}15\text{ }\mu\text{m}$, are characterized in terms of their transmission as a function of the electric field amplitude and the response times for switching into and out of the scattering state. The results show that the printed droplets, and arrays thereof, exhibit similar electro-optical properties to analogous thin-film devices, but with the ability to incorporate bespoke features such as images and decorative patterns. Finally, the electro-optical switching of a printed PSCLC privacy window whereby alphanumeric characters can be made to appear and disappear with the application of an electric field is demonstrated.

Liquid crystals (LC) have been particularly popular as the functional material used in smart window technologies because their optical characteristics can be altered either using applied electric fields or remotely using photo-illumination. The LC films that are typically employed often belong to one of the following classes: polymer stabilized LCs (PSLC),^[6] polymer dispersed LC (PDLC),^[7] or chiral nematic LC (CLC).^[8] Each of these systems can give rise to a light scattering state or a transparent state depending upon the material combination, device architecture, and electric field conditions. Polymer-stabilization has also been combined with CLCs (PSCLCs), as first introduced by Yang from Kent State University in 1992.^[9]

1. Introduction

Smart windows play an important role in managing energy consumption in buildings^[1] and automotive vehicles, particularly in environments that experience prolonged periods of extreme temperature conditions.^[2] These smart window technologies can help to maintain a comfortable temperature inside both buildings and vehicles whilst at the same time providing privacy features. Specifically, smart windows can prevent solar radiation from either entering or escaping the building depending upon the optical properties of the material used within the window pane.^[3] Additionally, spatially patterned smart windows can be fabricated with additional functionality such as the appearance of company logos/signage^[4] or the integration of temperature sensors.^[5]

A notable benefit of using PSCLCs in comparison to say PDLCs is that they can exhibit both a conventional mode (whereby the device switches from a scattering to a transparent state with an alternating current (AC) electric field) and reverse mode (switching from a transparent to scattering state) by simply changing the photopolymerization conditions rather than having to change the LC material (positive dielectric anisotropy LC for conventional mode^[10–11] and negative dielectric anisotropy LC for reverse mode^[12–13]). For example, if the PSCLC is photopolymerized while a voltage of sufficient amplitude is applied to the LC film then it can exhibit an opaque/light scattering state in the voltage off state. However, when a voltage is applied to the LC, the helical structure unwinds forming a nematic LC with a homeotropic alignment,^[9] which appears transparent. Alternatively, if the photopolymerization process takes place in the absence of an applied voltage then the off state is transparent (as determined by the alignment layer conditions) but the device becomes opaque/scattering when the LC is subjected to an external voltage. Spatially patterned PSCLCs have also attracted interest for numerous reasons and are typically patterned with the aid of a photomask.^[14] This process has been used to produce spatial features such as two-dimensional barcodes^[15] and temperature indicators.^[16] A drawback with this approach is that a new photomask is required every time the design is altered or modified. Moreover, achieving a high spatial resolution and complex pattern on-demand can be challenging.

Recently, we have used drop-on-demand (DoD) inkjet printing to spatially pattern polymer-dispersed LCs (PDLCs) and have employed this technique to demonstrate prototype smart windows with logos/emblems that can be switched off with the

M. Li, W. Kamal, A. C. J. Orr, A. A. Castrejón-Pita, S. J. Elston, S. M. Morris
Department of Engineering Science
University of Oxford
Parks Road, Oxford OX1 3PJ, UK
E-mail: stephen.morris@eng.ox.ac.uk

© 2022 The Authors. Macromolecular Chemistry and Physics published by Wiley-VCH GmbH. This is an open access article under the terms of the Creative Commons Attribution License, which permits use, distribution and reproduction in any medium, provided the original work is properly cited.

DOI: 10.1002/macp.202200154

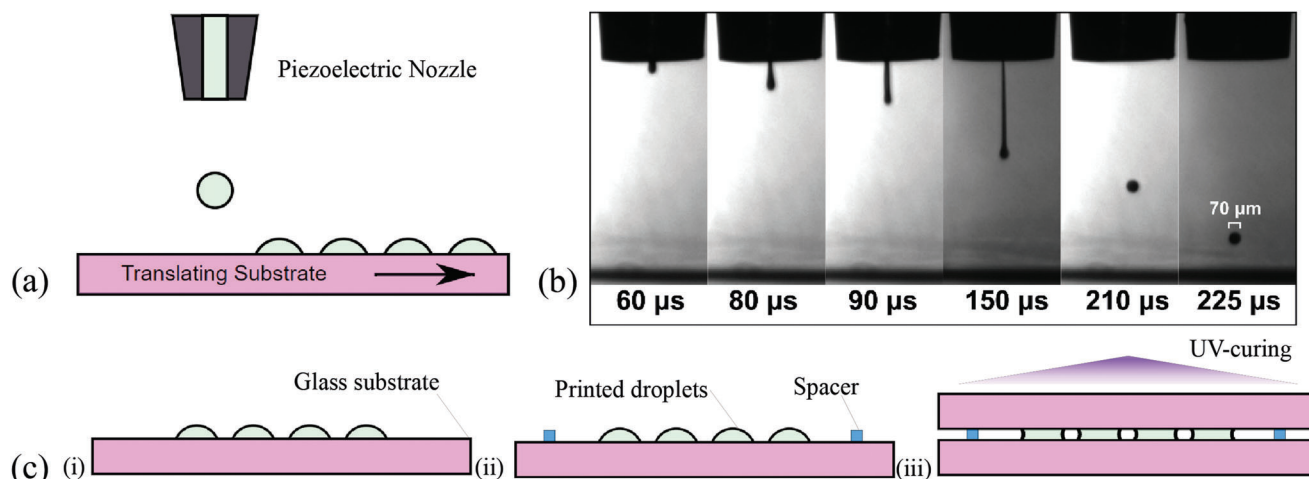


Figure 1. a) Inkjet printing process of the PSCLC mixture (93.5 wt% E7, 3 wt% BDH1281, 3 wt% RM257, and 0.5 wt% IR819). b) Shadowgraph images of the PSCLC droplet formation process with an 80 μm diameter print-head. For the printing process, the print head was held at a temperature of 68 $^{\circ}\text{C}$ to reduce the viscosity and surface tension of the LC ink. c) Illustration of the device fabrication process including: i) droplets loaded onto the substrate, ii) attachment of spacers, iii) attachment of the top ITO glass slide, and photopolymerization process.

application of an electric field.^[4] It is well-known that DoD printing is an efficient and high-precision technique that can be used to fabricate sophisticated and arbitrary patterns using advanced functional materials. However, a key limitation in our previous work is that for PDLCs with a positive dielectric anisotropy the transparent state is only accessible using an applied voltage. It would be highly beneficial if, using the same printed formulation, one could select either the conventional or reverse-mode functionality by simply changing the photocuring conditions.

Therefore, the aim of this paper is to report the development of conventional and reverse mode spatially patterned privacy windows fabricated using the DoD printing of a PSCLC ink. It is shown that printed patterns can be made to operate in either a conventional or reverse mode configuration depending upon the photopolymerization conditions. The electro-optical properties of printed droplets and arrays are presented and compared with those obtained for thin films formed using the same material combinations. Finally, printed PSCLC patterns are presented that demonstrate how images can be embedded into a PSCLC windowpane.

2. Results and Discussion

2.1. Electro-Optic Characteristics of Printed PSCLC Droplets

The printing and device assembly processes are illustrated schematically in **Figure 1**. Figure 1a shows an illustration of the deposition of individual picolitre volume droplets onto an indium tin oxide (ITO)-coated glass substrate using a DoD printing process with a piezoelectric-driven print-head and Figure 1b shows a sequence of shadowgraph images demonstrating the printing of individual PSCLC droplets that are free from jet break-up and satellite formation. Further information about the experimental procedures used to print the droplets is provided in the Experimental section. After printing, two spacers were attached to the edge of the substrate before another ITO glass slide was applied to form a top substrate (as illustrated in Figure 1c). Araldite rapid

epoxy adhesive was then used to fasten the glass slides together before the device was cured with ultraviolet (UV) light under different electric field conditions for the conventional and reverse modes.

For the conventional mode sample, the PSCLC was photopolymerized in the presence of an electric field above the critical electric field required for the chiral nematic-nematic transition to occur. After the photopolymerization process, and when the field was subsequently removed, the film tended to form a scattering state. To obtain a transparent state, an electric field (E) of $E = 6 \text{ V } \mu\text{m}^{-1}$ was applied to unwind the helix and to form a homeotropic nematic alignment whereby the director was aligned along the electric field direction. For this conventional mode sample, the mixture is in a focal conic state in the field-off configuration because the polymer network favors the homeotropic state, which prevents the Grandjean alignment from forming. Only when an electric field of a sufficient amplitude is reapplied will it become transparent again.

For the printed PSCLC device photopolymerized without the application of an electric field, on the other hand, a Grandjean texture (standing helix alignment) is obtained at $E = 0 \text{ V } \mu\text{m}^{-1}$. However, when an electric field of sufficient amplitude is subsequently applied the mixture transforms to a focal conic state, resulting in strong light scattering. This is called the reverse mode. If the electric field is then removed, the LC will relax back to the planar aligned (Grandjean) state, which appears transparent as long as the reflection band of the chiral nematic does not coincide with visible wavelengths, as is true for our samples.

Figure 2 presents the results of the electro-optical properties of a single printed PSCLC droplet operating in the conventional mode. For the conventional mode, with increasing field amplitude the focal conic (scattering) state switches to a homeotropic nematic LC resulting in a transparent state. The transmission as a function of electric field and time were obtained with the experimental setup presented in Figure S1, Supporting Information. Conventional and reverse mode thin-film devices are illustrated in Figure S2, Supporting Information. The diameter of the

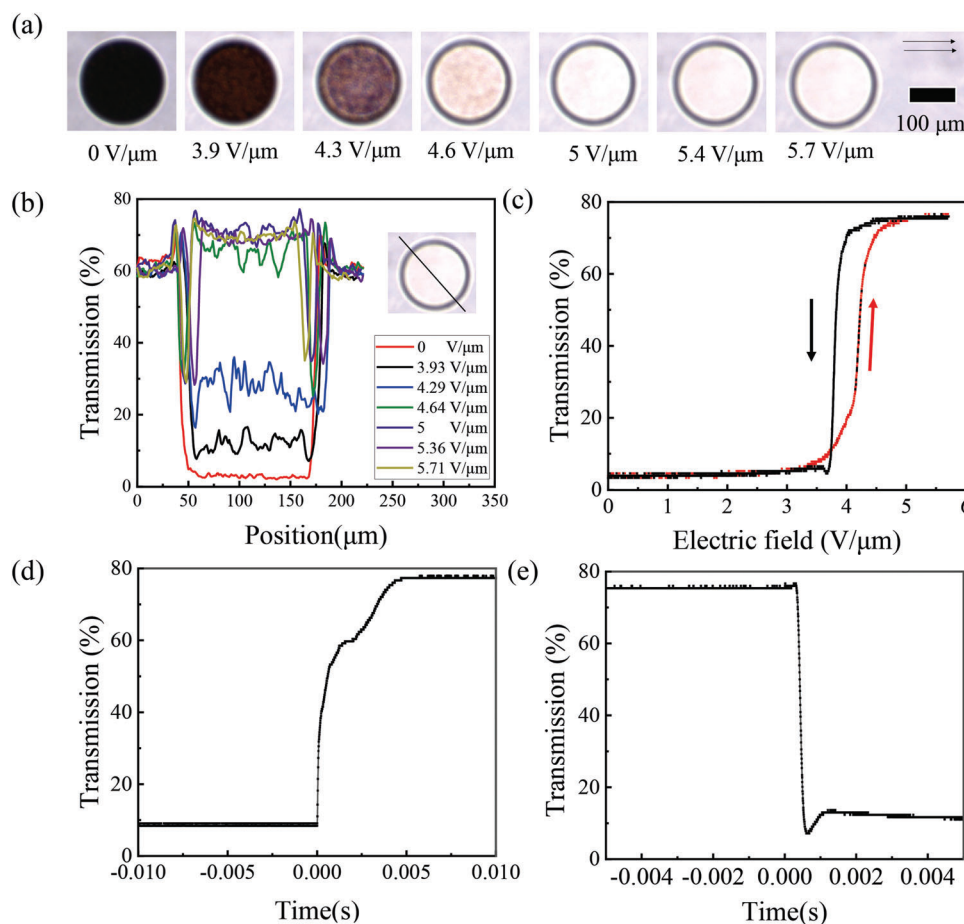


Figure 2. Electro-optic characteristics of a printed PSCLC droplet (93.5 wt% E7, 3 wt% BDH1281, 3 wt% RM257, and 0.5 wt% IR819) operating in the conventional mode (scattering to transparent). The droplet was printed at a temperature of 68 °C with an 80 μm diameter nozzle and photopolymerized in the presence of an electric field of $E = 5 \text{ V } \mu\text{m}^{-1}$ at 25 °C. The droplet diameter footprint was 190 μm (after device assembly) and the gap between the glass substrates was 14 μm . a) Polarizing optical microscope images of a printed PSCLC droplet observed between parallel polarizers (indicated by the single-headed black arrows). b) Line profile of a single printed PSCLC droplet at different electric field amplitudes. c) Transmission of a He-Ne laser through the printed PSCLC droplet as a function of electric field (for both increasing (red line) and decreasing (black line) amplitudes). Change in transmission as a function of time when the PSCLC droplet was switched on d) and then off e) with an electric field of $E = 5 \text{ V } \mu\text{m}^{-1}$. All measurements were carried out at a temperature of 25 °C.

droplet footprint in this case was ≈ 190 microns and the thickness of the device was $\approx 14 \mu\text{m}$. Figure 2a shows representative polarizing optical microscope (POM) images of a printed PSCLC droplet between parallel polarizers for different electric field amplitudes. In the absence of an applied field, the printed droplet adopted a focal conic state, scattering the light and leading to a dark appearance when viewed on the microscope.

When the electric field was increased to $E = 5 \text{ V } \mu\text{m}^{-1}$, the helical structure began to unwind as the director inside the droplet aligned with the electric field direction. In all cases, a ring was observed around the droplet that still scattered the light in spite of the applied electric field. This is due to the refraction/reflection of the light at the edge of the droplet, resulting in strong scattering. This effect is illustrated in Figure S3, Supporting Information. A line scan taken through the droplet in the POM images was then used to extract the transmitted intensity for a single printed droplet as the field was increased (Figure 2b). With increasing field amplitude, it can be seen that the transmission in the circu-

lar area that is defined by the droplet increases. For electric field amplitudes ranging from $E = 0$ –4.3 $\text{V } \mu\text{m}^{-1}$, the transmission remained low, and there was only a small change in the PSCLC configuration for this range of electric field amplitudes. However, upon increasing the amplitude to $E = 4.6 \text{ V } \mu\text{m}^{-1}$ there was a noticeable change in the transmission intensity (as can be seen in both (a) and (b)). For a further increase in the electric field amplitude ($E > 5 \text{ V } \mu\text{m}^{-1}$) the transmitted intensity across the droplet did not change significantly as can be seen in Figure 2b (e.g., from $E = 5$ –5.7 $\text{V } \mu\text{m}^{-1}$).

Figure 2c shows the results for the transmitted light intensity as a function of the electric field for both increasing and decreasing amplitude. Here an amplitude modulated signal was applied to the printed PSCLC droplet device to slowly increase the amplitude of the 1 kHz continuous square wave carrier signal. Upon increasing the amplitude of the electric field no change was observed until the amplitude reached approximately $E = 3.8 \text{ V } \mu\text{m}^{-1}$. Above this value, the transmission increased steeply

with a further change in the electric field amplitude, before it increased more gradually above $E = 4.7 \text{ V } \mu\text{m}^{-1}$ corresponding to an unwinding of the helix and the chiral nematic-nematic transition. These results are consistent with the results recorded on the microscope (Figure 2a) since they both showed a transparent state when the electric field was greater than $4.6 \text{ V } \mu\text{m}^{-1}$. Compared with the transmission of the transparent state of the film device (86%, Figure S4a, Supporting Information), the field-on homeotropic state transmission was found to be around 10% lower for the printed droplet device (76%). This is mainly due to the influence of device thickness, but it may also be due to scattering at the edges of the droplets, as well as potentially lower quality alignment in the printed droplets. For the data taken with a microscope (Figure 2b) the higher numerical aperture of the condenser and objective will also have an influence. However, for the printed droplet device, the contrast ratio (CR) improves by nearly a factor of five – being $\text{CR} = 3.2$ for the film device whereas $\text{CR} = 15.3$ for the printed droplet device. This is because the droplet device is much thicker than the film device, which then results in a strongly scattering state when there is no voltage applied.

Decreasing the electric field amplitude reveals that the transmission begins to decrease at an electric field of $E = 4.3 \text{ V } \mu\text{m}^{-1}$ as the helix begins to reform, and the onset of scattering begins. At an electric field of $E = 3.7 \text{ V } \mu\text{m}^{-1}$, the transmission reached its minimum value as the focal conic scattering state had been reformed. The results clearly show a degree of hysteresis in the switching when comparing the response for increasing and decreasing the magnitude of the applied electric field. For example, the transmission is midway between its maximum and minimum values at $E = 4.2 \text{ V } \mu\text{m}^{-1}$ on increasing the electric field amplitude, but this same value for the transmission was observed at $E = 3.8 \text{ V } \mu\text{m}^{-1}$ on decreasing the electric field amplitude. Hysteresis in the transmission was therefore observed when increasing and decreasing the field in accordance with previous studies.^[17–18]

Figure 2d,e shows the rise (scattering to transparent) and fall (transparent to scattering) times for the printed PSCLC droplet, respectively. These results were obtained when the printed droplet was subjected to a square wave signal with a 1 kHz frequency and an electric field of $5 \text{ V } \mu\text{m}^{-1}$, which as shown in Figure 2a–c result in the printed droplet becoming transparent. Here the rise time was found to take around 4 ms whereas the fall time was completed in approximately 2 ms. These response times are consistent with those obtained for equivalent thin film devices, which were 5 ms for the electric field on and 2.5 ms for the field off (see Figure S4, Supporting Information). In Figure 2d it can be seen that a two-stage switching process takes place. In the first stage, the helix is distorted when a voltage is applied, which is a relatively fast process. In the second stage, however, the director needs to overcome the helix to form a homeotropic nematic alignment, which takes a relatively long time in comparison. A similar two-stage switching process was observed in the thin-film device (Figure S4c, Supporting Information).

The results obtained here are within the range of switching times observed by other researchers, although there is very substantial variation in the switching times of polymer stabilized chiral LC devices reported previously, which range from tens of μs ^[19–20] to tens of ms^[9] for the rise time and tens of μs ^[19–20] to tens of ms^[21–22] for the fall time. The response time is highly in-

fluenced by the ratio of effective viscosity to the effective elastic constant of the LC host and chiral dopant, as well as the pitch.^[23] Shorter pitch chiral nematic LC mixtures could result in faster response times. Additionally, the cell gap also influences the response time since in thicker cells, where there is a larger number of chiral pitches across the cell, more time is needed to transfer from one state to another. Further, the polymer network density, morphology, and elasticity, will also strongly influence switching times. In general, the thin-film device and the printed droplet device exhibited similar electro-optic characteristics which indicates that the DoD printing fabrication process did not compromise or significantly alter the switching behavior.

Results for the electro-optic characteristics of a printed reverse mode PSCLC droplet device are presented in Figure 3. Figure 3a shows example POM images of a printed reverse mode PSCLC droplet viewed between parallel polarizers for a range of different electric field amplitudes. The droplet footprint diameter in this case was $205 \text{ } \mu\text{m}$ and the cell gap was $13 \text{ } \mu\text{m}$. The images show that with an increase in the electric field, the printed PSCLC droplet changed from a colored, polydomain Grandjean texture to a state that appears dark in the center of the droplet at $E = 1.6 \text{ V } \mu\text{m}^{-1}$. However, it was found that there was thin region around the circumference of the droplet which did not appear to change at this electric field amplitude. A further increase in the electric field resulted in the central region of the droplet becoming darker, which was also accompanied by a change in the appearance of the outer ring, with the droplet appearing completely black at around $E = 4.0 \text{ V } \mu\text{m}^{-1}$. This dark appearance is due to the incident light being strongly scattered by the droplet. As for the conventional mode, there was no apparent change in the droplet dimensions with the application of the electric field.

For the printed droplet, the Grandjean state was found to have more disclinations and defects when compared with an analogous thin film device. Despite the presence of these disclinations, the droplets still exhibited a relatively good contrast between the initial transparent state ($E = 0 \text{ V } \mu\text{m}^{-1}$) and the scattering state ($E = 4.0 \text{ V } \mu\text{m}^{-1}$). The disclinations that are observed are due to the imperfect alignment of the LC director in the Grandjean state. The texture can be further improved by optimizing the substrate treatment and/or the alignment layer. In future commercial applications, it will be possible to use more optimized alignment processes and hence reduce the influence of disclinations and defects on device performance. Additionally, it can be noted that some regions near the droplet edge do not switch fully. This may be due to some variation in the network formation in this area, for example, due to multiple refraction/reflection during UV curing, as illustrated in Figure S3, Supporting Information.

Again, hysteresis was observed upon increasing and decreasing the electric field amplitude (see Figure 3b). These results were obtained by slowly increasing the amplitude of a 1 kHz square wave carrier until it reached a maximum of $E = 4.6 \text{ V } \mu\text{m}^{-1}$. As the electric field amplitude increased, the Grandjean texture was distorted by the application of the field which resulted in the growth and formation of a focal conic state, as seen by the transparent to scattering transition. In contrast to the thin-film device, the lowest transmission value was observed at an electric field amplitude of around $E = 4 \text{ V } \mu\text{m}^{-1}$, which is slightly lower than that observed for the thin-film device. A further increase

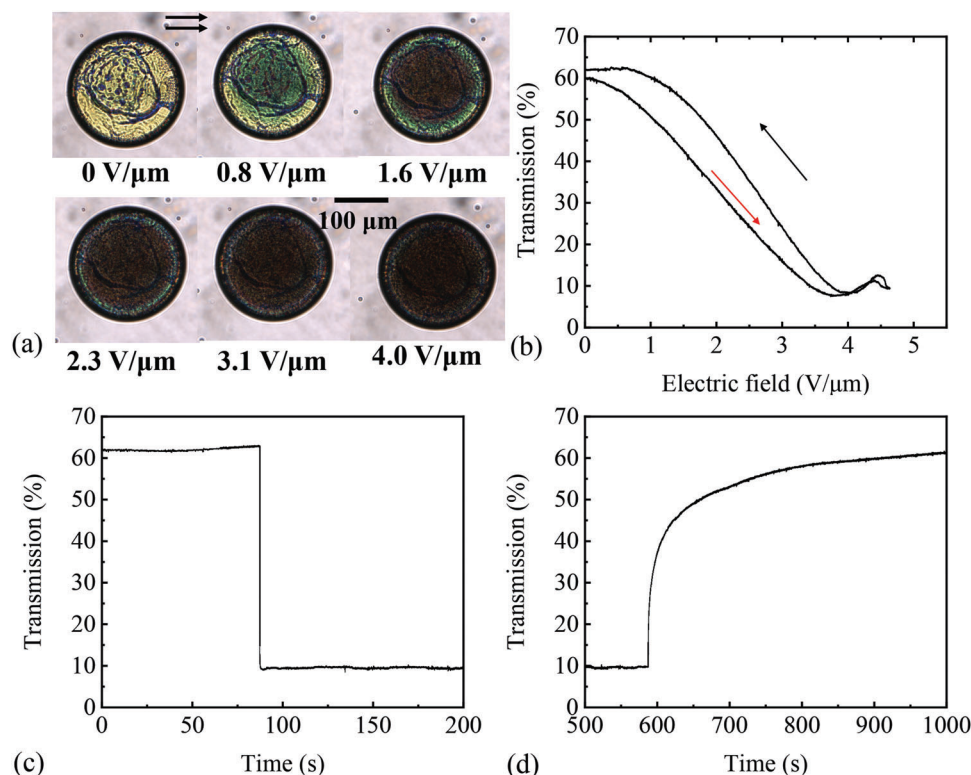


Figure 3. Electro-optic characteristics of a printed single PSCLC droplet (93.5 wt% E7, 3 wt% BDH1281, 3 wt% RM257, and 0.5 wt% IR819) operating in the reverse mode (transparent to scattering). The droplet was printed at a temperature of 68 °C and photopolymerized without an applied electric field at a temperature of 25 °C. The droplet diameter was 205 μm (after device assembly) and the gap between the glass substrates was 13 μm. a) Polarizing optical microscope images of a printed PSCLC droplet viewed with parallel polarizers (indicated by the single-headed black arrows). b) Transmission of a He-Ne laser through the PSCLC droplet as a function of the applied electric field amplitude (upon increasing (red line) and decreasing (black line) the amplitude). The change in transmission through the printed PSCLC droplet as a function of time when the PSCLC droplet was switched on c) and then off d) with an electric field of $E = 4 \text{ V } \mu\text{m}^{-1}$. All measurements were carried out at a temperature of 25 °C.

in the electric field leads to an unwinding of the helical structure as the strength of the field dominates over the twist induced by chirality, forming a second transmission state above the critical unwinding field. This phenomenon is much more obvious in the results presented for the thin-film device as shown in Figure S4b, Supporting Information whereby the transmission begins to increase for field amplitudes above $E = 5.4 \text{ V } \mu\text{m}^{-1}$. It is worth noting that this second transmission state is surplus to requirements for smart window applications. The highest transmission recorded was found to be $\approx 62\%$, which is around 10% lower than for the film device operating in the same mode (70%, Figure S4, Supporting Information). This is due to the thickness of the PSCLC layer combined with the imperfect alignment of the droplet in the Grandjean state. Different droplets may have some variation in texture, leading to some droplet-to-droplet variation in optical properties. The printed droplet device also shows a higher contrast ratio compared with the film device because of the influence of the thickness.

The response times for the printed reverse mode PSCLC droplet device were measured when a 1 kHz frequency square wave with an amplitude of $E = 4.0 \text{ V } \mu\text{m}^{-1}$ was applied across the printed PSCLC droplet and subsequently removed. Figure 3c,d show the rise time (transparent to scattering) and the fall time (scattering to transparent), respectively. In this case, the response

time for the field on process was found to be 10 ms, but approximately 400 s for the field off process.

The dynamic response times recorded here for the field off process are notably different from that recorded for the thin film device (see Figure S4, Supporting Information). One possible reason might be that the printed droplet device was much thicker (by approximately a factor of three) than the thin-film device. The factors that govern the restoration of the standing helix configuration are the surface alignment conditions and the polymer network that was formed in the Grandjean state. Consequently, it is expected that thicker devices result in a slower relaxation process in terms of the recovery of a uniform Grandjean state upon removal of the applied electric field.

Overall, for the reverse mode window, the LC mixture needs to be pre-aligned by the surface alignment to form the Grandjean state. However, in the conventional mode the LC mixture does not require any pre-alignment. In the transparent state, the reverse mode smart window is in the Grandjean state whereby the LC director aligns parallel to the substrate. Therefore, the transmission of the smart window in this state highly depends on the alignment of the LC director. On the other hand, for the LC device operating in the conventional mode, the transparent state occurs when the voltage is applied, which forces the LC director to be perpendicular to the substrate. This means that the different

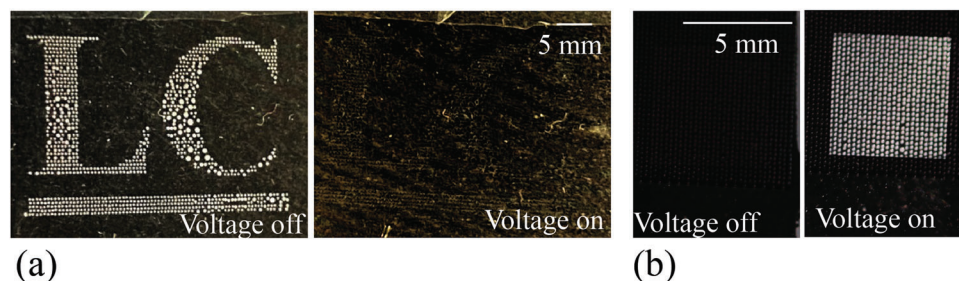


Figure 4. Printed patterns and arrays of PSCLC droplets (93.5 wt% E7, 3 wt% BDH1281, 3 wt% RM257, and 0.5 wt% IR819) operating in a) conventional mode and b) reverse mode. The droplets were printed at a temperature of 68 °C with an 80 μm nozzle and photopolymerized at 25 °C with an electric field of $E = 5 \text{ V } \mu\text{m}^{-1}$ for a) and without an electric field for b). The cell gap of the two devices was 10 μm (conventional mode) and 8 μm (reverse mode). The droplet diameters were all approximately 110 μm .

states of the LC director then result in some difference in the behavior of the transmittance.

2.2. Printed PSCLC Arrays and Windows

After successfully identifying the conditions for printing droplets of a PSCLC mixture and characterizing their electro-optic properties, spatial features such as arrays can be printed by digitally printing multiple droplets across the substrate. This was achieved using the scripting language provided by the Jetlab-II printing system, which can generate arrays and circles, as well as print representations of raster images. Such a system could therefore print customized logos, signs, or text. Here we show a window with the letters “LC” (Figure 4a) operating in the conventional mode. The device was fabricated with the same PSCLC ink formulation and the same printing parameters as shown for the single droplet case in Figure 2, and the cell gap was 10 μm . It can be clearly seen that the printed droplets scatter light when there is no voltage applied, and so the letters can be seen, while for an applied electric field the droplets become transparent and the letters disappear. Using the same printing parameters, a square array of 25×25 droplets was printed on polyimide-coated ITO glass slides and photopolymerized without any electric field to create a reverse mode sample. The results are shown in Figure 4b. The cell gap in this case was 8 μm .

Some regions show variation in droplet sizes in Figure 4. This is caused by the top electrode assembly process, when the two electrodes are brought together with a certain amount of pressure, resulting in slight non-uniformities and unevenness which can cause some of the droplets to merge together. In a commercial process this can be improved by using a highly uniform distributed pressure for the assembly process, together with distributed spacer-beads to lead to very well-regulated cell gap control. These combined results indicate that this mixture and density of the droplets are suitable for a switchable design. Additionally, the printing process can be automatically controlled, and the patterns can be printed in different designs. Using commercial printing processes, this can be further developed to produce large-area switchable patterns and images.

To the best of our knowledge, this is the first report of inkjet printing of a PSCLC mixture for the fabrication of smart windows that can undergo both conventional mode and reverse mode switching. The benefit of printing such windows lies in the flex-

ibility in the design, which can produce intricate patterns/logos with excellent print resolution. These printed smart windows are particularly suited to modern architectural design features where they can serve the purpose of being both aesthetically pleasing and energy-saving by controlling the amount of light that is transmitted into or out of a building.

3. Conclusion

In summary, we have used drop-on-demand (DoD) inkjet printing to fabricate polymer-stabilized chiral nematic liquid crystal (PSCLC) privacy windows that can be made to operate in either a scattering (reverse) mode by changing the photopolymerization conditions. On the whole, the electro-optic characteristics observed for the printed droplets operating in either mode were found to be comparable to those recorded for the corresponding thin film devices. The one difference was that the fall-time of the printed reverse mode droplets was significantly longer than that recorded for the thin-film devices; this is believed to be due to the difference in the thickness of the printed droplet and thin-film devices. Printed arrays of PSCLC droplets provides complete freedom of design in terms of the patterning that can be achieved, and this has been used to fabricate demonstrative privacy panels operating in either mode. Specifically, in this work, we have used printed alphanumeric characters to demonstrate that they can be made to disappear with the application of an electric field for the conventional mode and that a printed square array can be made to appear with an electric field for the case of the reverse mode. We believe that the approach presented in this work provides a route toward the fabrication of versatile and bespoke privacy panels that can display images and signage without the need for photomasks and complex lithography processes.

4. Experimental Section

Materials and ink preparation: In this work, the room-temperature nematic LC mixture, E7, (obtained from Synthon Chemicals Ltd) was used without further purification. The ordinary and extraordinary refractive indices of the nematic LC are reported to be $n_o = 1.52$ and $n_e = 1.74$, respectively, at a wavelength of 633 nm and a temperature of 20 °C. The high twisting power chiral dopant, BDH1281 (Merck), was added to the nematic LC at a low concentration by weight (3 wt.%) to form a chiral nematic LC. A diacrylate reactive mesogen, 1,4-Bis[4-(3-acryloyloxypropyloxy)

benzoyloxy]-2-methylbenzene (RM257 from Synthron Chemicals Ltd) was used in combination with a photoinitiator, IR819 (Ciba-Geigy) in order to form a polymer network inside the chiral nematic LC layer when exposed to ultraviolet (UV) light. Specifically, the mixture used in this study was composed of 93.5 wt.% E7, 3 wt.% BDH1281, 3 wt.% RM257, and 0.5 wt.% IR819. This formulation was thermally and mechanically mixed at a temperature of 68 °C with a magnetic stirrer at a speed of 300 rpm for 24 h. This temperature was above the clearing point at which the nematic E7 becomes an isotropic liquid, which is 58 °C. The mixture was found to result in a chiral nematic LC with a right-handed helical structure with a reflection band with a central wavelength at 859 nm. The pitch of the PSCLC mixture was measured to be $p = 533$ nm (from the transmission spectrum of white light in the Grandjean state) and the helical twisting power (β) of the chiral dopant in this mixture was estimated to be $\beta \approx 63 \mu\text{m}^{-1}$.

PSCLC droplet device fabrication: The spatially patterned printed devices were fabricated using ITO coated glass slides (Ossila). The ITO slides were left untreated for the conventional mode device fabrication. For the reverse mode devices, which require a Grandjean (standing helix alignment) in the field off state, the ITO slides were coated with a 5% Polyvinyl Alcohol (PVA) water solution and then dried in an oven for around 2 min to form a thin layer of PVA. A rubbing machine was then used to align the PVA layer, resulting in a uniform homogeneous alignment of the LC.^[24]

The printing process was accomplished using a Jetlab-II printing system (MicroFab Technologies Inc), which includes a three-axis translation stage and multiple piezoelectric printheads in a heating module (Eurotherm 2408i). The internal diameter of the printhead's nozzle used was 80 μm (MicroFab MJ-AT-01-80). Backpressure of the printhead was provided by a computerized pneumatic system and used to control the unperturbed liquid meniscus at the nozzle and to ensure that the dispenser was fully filled with the PSCLC material before printing.

For the printing process, the printhead was heated to a temperature of 68 °C to lower the viscosity and surface tension of the PSCLC ink, which ensured a stable jetting process without satellite droplet formation. To observe droplet formation and the printing process, as well as the impact with the substrates, a camera (Omron Sentech STC-MB33USB T&L0203) integrated inside the printing system was used. Arrays of single droplets were printed to form recognizable spatial patterns, for example, grids and a logo.

For the conventional mode (scattering to transparent state), the mixture was photopolymerized in the presence of a voltage of 70 Vrms (corresponding to an electric field (E) of $E = 5 \text{ V}\mu\text{m}^{-1}$) that locks-in a scattering state even once the voltage had been removed. The power density of the UV light ($\lambda = 365$ nm) source (CS2010, Thorlabs) used to photopolymerize the LC mixture was 27 mW cm^{-2} for 3 min.^[25] These photopolymerization conditions were used based upon a previous study, where it was found that this power density and exposure time resulted in a desirable scattering state.^[25] The power density was monitored with a handheld power meter (PM100D, Thorlabs) attached to a photodiode (S120VC, Thorlabs). In contrast, for the reverse mode device (transparent to scattering state), the sample was photopolymerized with the same UV power density and duration, but with no applied electric field. This resulted in a Grandjean alignment in the absence of an electric field after fabrication. All steps up to the photopolymerization process were carried out under the illumination of yellow light to prevent premature photoinduced polymerization.

Characterization: All samples were observed on an Olympus BX51 polarizing optical microscope in transmission mode at various magnifications (4x, 10x, 20x). For the measurement of the transmission and scattering characteristics, as well as the response times, a He-Ne laser (JDS Uniphase, 1122P) was used ($\lambda = 633$ nm) to illuminate the PSCLC samples so that the transmitted light could be determined. The transmitted light was detected using a photodiode (Thorlabs PDA36A-EC SI Amplified Detector). In order to generate amplitude modulated (AM) signals to drive the PSCLC films and printed droplets, two function generators (Multicomp Pro MP750065) were used in combination, with the output of one connected to the AM input of the other. Finally, an oscilloscope (Tektronix TDS2004B) was used to capture and display the response recorded by the photodiode.

Supporting Information

Supporting Information is available from the Wiley Online Library or from the author.

Acknowledgements

W.K. acknowledges the financial support provided by Punjab Educational Endowment Fund (PEEF), Pakistan. A.C.J.O. acknowledges the Engineering and Physical Sciences Research Council for a graduate studentship (EP/R513295/1). A.C.P. acknowledges the John Fell Fund (Oxford University Press) through Project No. 0005176 to provide matching funds to acquire the JetLab II system.

Conflict of Interest

The authors declare no conflict of interest.

Data Availability Statement

The data that support the findings of this study are available from the corresponding author upon reasonable request.

Keywords

chiral nematic liquid crystals, inkjet printing, polymer stabilization, smart windows

Received: May 12, 2022
Revised: August 2, 2022
Published online: August 19, 2022

- [1] Y. Ke, C. Zhou, Y. Zhou, S. Wang, S. H. Chan, Y. i Long, *Adv. Funct. Mater.* **2018**, *28*, 1800113.
- [2] Y. Ke, J. Chen, G. Lin, S. Wang, Y. Zhou, J. Yin, P. S. Lee, Y. Long, *Adv. Energy Mater.* **2019**, *9*, 1902066.
- [3] S. Nundy, A. Mesloub, B. M. Alsolami, A. Ghosh, *J. Cleaner Prod.* **2021**, *301*, 126854.
- [4] W. Kamal, M. Li, J. D. Lin, E. Parry, Y. Jin, S. J. Elston, A. A. Castrejón-Pita, S. M. Morris, *Adv. Opt. Mater.* **2022**, *10*, 2101748.
- [5] Y. Guo, H. Shahsavan, M. Sitti, *Adv. Opt. Mater.* **2020**, *8*, 1902098.
- [6] A. Y. G. Fuh, S. Y. Chih, S. T. Wu, *Liq. Cryst.* **2018**, *45*, 864.
- [7] D. Cupelli, F. P. Nicoletta, S. Manfredi, M. Vivacqua, P. Formoso, G. De Filipo, G. Chidichimo, *Sol. Energy Mater. Sol. Cells* **2009**, *93*, 2008.
- [8] C.-W. Chen, A. N. Brigeman, T.-J. Ho, I. C. Khoo, *Opt. Mater. Express* **2018**, *8*, 3.
- [9] D.-K. Yang, L.-C. Chien, J. W. Doane, *Appl. Phys. Lett.* **1992**, *60*, 3102.
- [10] A. K. Jain, R. R. Deshmukh, in *Liquid Crystals and Display Technology*, IntechOpen, London **2020**, *2*, 11.
- [11] M.-Y. Chen, J.-Y. Lee, *J. Chin. Inst. Eng.* **2014**, *37*, 793.
- [12] V. Sharma, P. Kumar, Chinky, P. Malik, K. K. Raina, *J. Appl. Polym. Sci.* **2020**, *137*, 48745.
- [13] S.-H. Hwang, K.-J. Yang, S.-H. Woo, B.-D. Choi, E.-H. Kim, B.-K. Kim, *Mol. Cryst. Liq. Cryst.* **2010**, *470*, 163.
- [14] X. Li, X. Du, P. Guo, J. Zhu, W. Ye, Q. Xu, Y. Sun, *Polymers (Basel)* **2018**, *10*, 884.
- [15] W.-S. Li, Y. Shen, Z.-J. Chen, Q. Cui, S.-S. Li, L.-J. Chen, *Appl. Opt.* **2017**, *56*, 601.
- [16] R. A. M. Hikmet, R. Polesso, *Adv. Mater.* **2002**, *14*, 502.

- [17] Y. H. Lin, H. Ren, Y.-H. Fan, Y.-H. Wu, S.-T. Wu, *J. Appl. Phys.* **2005**, *98*, 043112.
- [18] R. Yamaguchi, K. Goto, S. Sakurai, L. Xiong, T. Tomono, *J. Photopolym. Sci. Technol.* **2015**, *28*, 319.
- [19] D. J. Gardiner, S. M. Morris, F. Castles, M. M. Qasim, W. - S. Kim, S. u S. Choi, H. - J. Park, I. J. Chung, H. J. Coles, *Appl. Phys. Lett.* **2011**, *98*, 263508.
- [20] S. M. Morris, D. J. Gardiner, F. Castles, P. J. W. Hands, T. D. Wilkinson, H. J. Coles, *Appl. Phys. Lett.* **2011**, *99*, 253502.
- [21] G. Pan, L. Yu, H. Zhang, J. Guo, R. Guo, H. Cao, Z. Yang, H. Yang, S. Zhu, *Liq. Cryst.* **2008**, *35*, 1151.
- [22] K.-H. Chang, V. Joshi, L.-C. Chien, *Phys. Rev. E* **2017**, *95*, 042701.
- [23] G. Tan, Y.-H. Lee, F. Gou, H. Chen, Y. Huang, Y. F. Lan, C.-Y. Tsai, S.-T. Wu, *J. Phys. D: Appl. Phys.* **2017**, *50*, 493001.
- [24] K. Ha, J. L. West, *Liq. Cryst.* **2010**, *31*, 753.
- [25] X. Hu, X. Zhang, W. Yang, X.-F. Jiang, X. Jiang, L. T. Haan, D. Yuan, W. Zhao, N. Zheng, M. Jin, L. Shui, A. P. H. J. Schenning, G. Zhou, *J. Appl. Polym. Sci.* **2020**, *137*, 48917.